

# CMOS APS MTF Modeling

Igor Shcherback, Orly Yadid-Pecht, *Senior Member, IEEE*

Electrical Engineering Department  
Ben-Gurion University  
P.O.B. 653 Beer-Sheva 84105, ISRAEL

**Abstract**--In this work, a unified model, based on a thorough analysis of experimental data, is developed for the overall Modulation Transfer Function (MTF) estimation for CMOS image sensors. The model covers the physical diffusion effect together with the influence of the pixel active area geometrical shape.

Comparison of both, our predicted results and the MTF calculated from the Point Spread Function (PSF) measurements of an actual pixel array gives excellent agreement. This confirms the hypothesis that the active area shape together with the photocarrier diffusion effect are the determining factors of the overall CMOS Active Pixel Sensor (APS) MTF behavior, and allows us to extract the minority-carrier diffusion length.

The results indicate that for any potential active area shape, a reliable estimate of image performance is possible, so the trade off between the conflicting requirements, such as signal-to-noise ratio (SNR) and MTF could be compared per each pixel design.

**Index terms**—CMOS image sensor, Modulation Transfer Function (MTF), Point spread Function (PSF), diffusion process, parameter estimation, modeling.

## 1. INTRODUCTION

Solid-state imagers are based upon rectangular arrays of light-sensitive imaging sites, which are also called picture elements or pixels. In CMOS Active Pixel Sensor (APS) arrays, the pixel area is constructed of two functional parts (see for example, Fig. 1). The first part, that has a certain geometrical shape, is the sensing element itself: the active area that absorbs the illumination energy within it and turns that energy into charge carriers. APSs usually consist of photodiode or photogate arrays [1,2,3,4,5,6] in a silicon substrate. Each imaging site has a depletion region of several micrometers near the silicon surface. Any photocarrier generated in this depletion region is collected at this imaging site (we assume perfect collection efficiency for carriers at or within the depletion region). The second part is the control circuitry required for readout of this charge. The ratio between the active area and the total pixel area is

referred as the Fill Factor (FF), which in APS is less than 100 percent (in contrast to CCDs where the FF can approach 100%). The preferred shape of the pixel active area is a square. However, designing the active area as a square can reduce the fill factor. Since the fill factor influences the signal and SNR, it is preferred to keep it as high as possible. Fig. 1 describes an L-shaped active area pixel, which is most commonly used.

Fig. 1. –

Photon absorption in the silicon depends on the absorption coefficient  $\alpha$ , which is a function of the wavelength. Blue light, with wavelength  $\lambda \approx 0.4\mu m$ , is strongly absorbed in the first few micrometers of silicon, since  $\alpha$  is large in this spectral region. Longer wavelengths,  $\lambda \approx 0.6\mu m$ , for instance, have a smaller absorption coefficient, which means more of the photocarriers can be generated outside the depletion regions. These carriers diffuse to the original imaging site or to a nearby site where they are collected, before they are lost to a bulk recombination process. The imagers lose resolution as the result of this diffusion process. Fig. 2 shows a schematic cross section of several imager sites, which indicates the depletion-region boundaries.

Fig. 2. –

Theoretical calculations to model the effects of the photogenerated minority carriers spatial quantization, transfer efficiency, and crosstalk in CCDs have been described over the years [7, 8, 9, 10, 11, 12, 13, 14]. It has always been assumed that the theoretical model includes the solution of the two-dimensional continuity equation

$$D\nabla^2 n + \frac{n(x, z)}{\tau} = Nf(x, z)\alpha \exp[-\alpha z] \quad (1)$$

where  $n$ ,  $n(x, z)$  represents the minority carriers concentration,  $Nf(x, z)$  is the flux, transmitted to the substrate of the sensor at some position  $x$ ,  $\alpha$  is the absorption coefficient,  $z$ - the depth within the semiconductor,  $\tau$  - the minority carrier lifetime and  $D$ -the diffusion coefficient. It was already shown [9], that the multiplication of the diffusion and aperture Modulation Transfer Function (MTF) in purpose to arrive at the overall sensor MTF is only valid for the special case in which the pixel aperture

is equal to its size or pitch, i.e., for the case of a 100% fill factor. In other words, the unification of these effects is necessary for the right MTF representation.

It was recently shown that the active area shape contributes significantly to the behavior of the overall MTF of a CMOS imager [15]. This current work is a continuation of the formerly presented analytical analysis. Here we present a more comprehensive model, which takes into account the effect of the minority carrier diffusion together with the effect of the pixel active area shape on the overall CMOS-APS MTF. This is especially important for APS design, where the fill factor is always less than 100%.

Section 2 presents the details of the experimental measurements and the data acquisition method. Section 3 describes the physical analysis performed on the acquired data. It contains the fitting description and the relevant parameter derivation methods. Section 4 presents a computer model, which empirically produces the PSF of the pixel, using the previously described analysis. The comparisons between the modeled and actually scanned results are discussed in Section 5. Section 6 summarizes the work.

## 2. EXPERIMENTAL DETAILS

Our model is based on the measurements of responsivity variation on a subpixel scale, for the various APSs. These measurements were reported in [15] and will be described here briefly. An optical spot of size  $\approx 0.5\mu m$  (He-Ne laser,  $\lambda = 0.6\mu m$ ) was used to scan the APS over a single pixel and its immediate neighbors in a raster fashion step. The present paper deals with the ideal situation, where light is projected directly onto the sensor pixel. Therefore, effects on MTF due to the presence of an optical stack of oxides such as light-piping [16] are not considered. In addition, the spot size of the used laser is small compared with the pixel size; therefore, the effects of laser spot profile on the measured PSF are not considered.

The data acquisition was taken at the center point, i.e., the central pixel was read out at each point of the scan (see Fig.3). The obtained signal as a function of the spot position provides a map of the pixel response.

Fig. 3. -

Assume only the central pixel is active. The “window region” i.e., the photodiode (or photogate) of the active pixel is the only region where the wide (nonzero bias) depletion layer exists and the photocarrier

collection occurs. The incoming laser light generates (at a certain depth according to the exponential absorption law) electron-hole pairs i.e., minority charge carriers. Part of these carriers diffuse (with equal probability to all directions) directly to the depletion region, where they subsequently contribute to the resultant signal. Thereby, the resulting PSF we obtain in the window region (see Fig.4) consist of the detection of those charge carriers, which successfully diffused to the depletion region. The value at each point represents the electrical outcome of the three-dimensional photocarrier diffusion (i.e., the integration over the depth at each point) from this point to the depletion. Thus, the 2D signal map plane we get in the experiment can be generally considered as a “diffusion map” of the 3D diffusion in the device. In Fig. 4 the lighter the gray level, the stronger the response.

Fig. 4. –

### 3. PHYSICAL ANALYSIS

We perform an analysis of the PSF obtained from the actual pixel measurements for a square, a rectangular, and an L-shaped active area by means of a scientific analysis software. Note that without the limitation of generality, in this work we demonstrate, as an example, only the results for an L-shaped active area pixel. We use the solution of the steady-state one-dimensional transport equation of excess minority carriers in the semiconductor

$$\frac{\partial n_p}{\partial t} = -\frac{n_p - n_{p0}}{\tau_n} + D_n \frac{\partial^2 n_p}{\partial x^2} \quad (2)$$

where the electron recombination rate can be approximated by the expression  $(n_p - n_{p0})/\tau_n$ , where  $n_p$  is the minority carrier density,  $n_{p0}$  - the thermal equilibrium minority carrier density,  $\tau_n$  - the electron (minority) lifetime, and  $D_n$  - the electron diffusion coefficient. The solution is given by:

$$n_p(x,t) = \frac{N}{\sqrt{4\pi D_n t}} \exp\left[-\frac{x^2}{4D_n t} - \frac{t}{\tau_n}\right] + n_{p0} \quad (3)$$

where  $N$  is the number of electrons generated per unit area (in a certain depth within the semiconductor).

Based on this solution we fit the PSF data acquired from the actual scanning. For each scanned pixel a set of fittings is performed. Fig. 5 indicates examples of planes on which fitting was performed for the L-shaped pixel (  $A'A''$  is one of the cross-sections a fit was performed on).

Fig. 5. -

All the pixels are situated on a common substrate. Therefore, for a given pixel array the photocarrier diffusion behavior within the substrate is common too. From the generalization of the fitting results for all pixels, we derive the common functional dependence with common parameters that describe the diffusion process in the array. The two-dimensional approach described earlier allows us to obtain the desired physical parameters, which correspond to the actual three-dimensional diffusion.

The model used for fitting, is

$$y = y_0 + \frac{A}{W \sqrt{\frac{\pi}{2}}} \exp\left[-\frac{2(x-x_c)^2}{W^2} - 1\right] \quad (4)$$

where  $X_c$  - is the center,  $W$  - the width,  $A$  - the area. The term “-1” describes the case of  $\tau=t$ . Obviously, it is generally possible to perform fittings with values of  $t$  equal to various fractions of  $\tau$ , so that for each window shape we obtain the best correspondence. We derive the relevant parameters from the comparison of equations 3 and 4

$$W = 2\sqrt{2D_n\tau}, \Rightarrow L_{\text{eff}} = \sqrt{D_n\tau} \quad (5)$$

where  $L_{\text{eff}}$  - is the characteristic effective diffusion length. The common average result we obtain for it is:  $L_{\text{eff}} \approx 24\mu\text{m}$ .

Fig. 6 describes the fit function and the actual data for one cross-section example.

Fig. 6. -

#### 4. THE UNIFIED MODEL DESCRIPTION

Based on the described analysis of the experimental data and the actual layout of the pixel array a unified numerical model including both the effect of photocarrier diffusion within the substrate and the

effect of the pixel sampling aperture shape and size within the pixel array is worked out. The model empirically produces the PSF of the pixel. We use the extracted parameters for the creation of a 2D symmetrical kernel matrix (there is no diffusion direction priority within the uniform silicon substrate). The convolution of this matrix with the one representing the pure geometrical active area shape produces the desired unified PSF model. The dimensions of the kernel matrix are important.

Fig. 7 below explains the choice of the kernel matrix dimensions. It could be seen that at the points corresponding to the kernel dimension, i.e. points 7~9, the mean and standard deviation functions obtained from the comparison between the modeled and the actually scanned PSF reach an extremum.

Fig. 7. –

These matrix dimensions (both) equal the physical pixel size in our representation. Thus, we conclude that the diffusion primarily occurs within the pixel, i.e.,  $L_{\text{eff}} \approx 24.4\mu\text{m}$ . Note that the parameter value obtained here directly from our model is the same as the one previously obtained analytically by fitting.

We present the experimental results and compare them with our predictions for several practical designs. It can be seen that, generally, we achieve a fair correspondence of the simulated PSF with the real, measured PSF. A thorough results discussion follows hereby.

## 5. RESULTS AND DISCUSSIONS

To compare the PSF and the MTF of a practical square, rectangular and an “L” active area shaped pixels, two-dimensional MTF of these structures for a specific design were calculated, simulated, and compared with the measurements. The measurements currently used for the analysis are from an HP  $1.2\mu$  process chip as described in [15]. The design consists of an APS sensor with different shaped pixel active areas:

1) a square shaped active area design with a fill factor of around 8%, 2) a rectangular shaped active area with a fill factor of 31%, 3) an “L” shaped design with a fill factor of around 55%. The square shape dimensions were  $11\lambda \times 11\lambda$ . The rectangular shape dimensions were  $35\lambda \times 14\lambda$ . The pitch was  $40\lambda$ , i.e.  $24.4\mu\text{m}$ . An example for the L-shaped layout is shown in Fig 1. Fig. 4 shows the corresponding Point Spread Function (PSF) map obtained by laser scanning in subpixel resolution (after [15]). Fig. 8 shows the

corresponding calculated MTF, via the 2D Fourier transform. In addition to the MTF results presented in [15] Fig. 9 represents the PSF map obtained from the unified computer model, and Fig. 10 shows the corresponding MTF contour plot. Fig. 11a and Fig. 11b show the comparison results. The first one (Fig. 11a) represents the difference between the actually measured PSF and the pure geometrical PSF (i.e., the PSF resulting from the active area geometrical pixel layout [15], represented by the unity in the active area and zero otherwise) for a specific pixel. The maximum difference observed is about 20% of the maximum pixel response. The second one (Fig. 11b) is the comparison between the actually measured PSF and the PSF obtained from our unified model, i.e., with the diffusion effects. The maximum difference observed is about 3% of the maximum pixel response. The histograms corresponding to the differences obtained in Figs. 11a and 11b are represented in Figs. 12a and 12b. The horizontal axis represents this difference as part of the maximum response (which is normalized to unity).

Fig. 8. –

Fig. 9. –

Fig. 10. –

Fig. 11. –

Fig. 12. –

The comparison of the extracted diffusion length values, presented in Table 1, gives a confirmation for the universality of the described method. Note that the calculation performed is based on the data extracted from the literature sources, relevant to the process described. The same model can be used for any process design.

Table 1. –

As was already shown [15], the active area shape contributes significantly to the behavior of the overall MTF. However, there are essential differences between the actual and geometrical MTFs. Our unified model gives better agreement between the modeled PSF/MTF for a certain active area shape and the actual measurements. One still can see (Fig. 11b) some difference between the PSF matrices, the one

actually scanned, and the one modeled. However, these differences are confined by the background level, and in average are calculated to be less than 1% (see the histogram on Fig. 12b). Those distinctions occur due to other factors in the design and process, such as optical crosstalk [17]. Optical crosstalk results from the interference in the oxide level, especially between metal lines, and has an effect on the overall MTF [8,9,10]. This would have more effect as the pixel size scales in multi-level metal processes [18]. In addition, the effects of the laser spot profile (used for scanning) on the resulting PSF should also be considered for smaller pixels, i.e., as the technology scales.

## 6. SUMMARY

In this work, analysis of experimental data of subpixel scanning sensitivity maps for pixel arrays with a different active area shape was performed. Based on this analysis, a unified model for estimating the MTF of a CMOS-APS solid-state image sensor was developed. This model includes the effects of the photocarrier diffusion within the substrate in addition to the effects of the pixel sampling aperture shape and size.

Minority-carrier diffusion length, characteristic for the process, was extracted for various active area pixels via several different ways. The agreement between the values obtained by the model and other methods verifies the usefulness of the model.

Comparison of both, the simulation results and the MTF calculated from the Point Spread Function measurements of the actual pixels confirms that the active area shape, in aggregation with the minority charge carrier diffusion effect, are the two determining factors which affect the overall MTF behavior.

The results also indicate that for any potential pixel active area shape, a reliable estimate of the degradation of image performance is possible, so that the tradeoff between conflicting requirements, such as signal-to-noise ratio (SNR) and MTF, could be compared per each pixel design for better overall sensor performance. The proposed model is general in nature. However, evolving technologies will cause other effects like wave-guides to become stronger and have more influence.

## ACKNOWLEDGEMENTS

The authors would like to thank the Israeli Ministry of Science and Technology and the Israeli Ministry of Trade for funding this project. In addition, we would like to thank Prof. Nissim Ben-Yosef for fruitful discussions.

## REFERENCES

- [1] E. R. Fossum, "CMOS Image Sensors: Electronic Camera on A Chip," *IEEE Trans. Electron Devices*, vol. 44, pp. 1689-1698, Oct 1997.
- [2] P. Bhattacharya, "Semiconductor Optoelectronic Devices," Prentice Hall, 1993.
- [3] N. S. Kopeika, "A System Engineering Approach to Imaging," SPIE Press, 1998.
- [4] K. M. Kramer, W. N. Hitchon, "Semiconductor Devices A Simulation Approach," Prentice Hall, 1997.
- [5] S. M. Sze, "Physics of Semiconductor Devices," New York, J. Wiley and Sons, 1981.
- [6] T. Spirig, "Smart CCD/CMOS based image sensor with programmable real time temporal, and spatial convolution capabilities for application in machine vision and optical metrology," ETH, Dissertation #11993, Switzerland.
- [7] T. O. Körner and R. Gull, "Combined Optical/Electric simulation of CCD Cell structures by Means of the Finite-Difference Time-Domain Method," *IEEE Trans. Electron Devices*, vol. 47, ED-5, pp. 931-938, May. 2000.
- [8] J. P. Lavine, E. A. Trabka, B. C. Burkey, T. J. Tredwell, E. T. Nelson, C. N. Anagnosyopoulos, "Steady-State Photocarrier Collection in Silicon Imaging Devices," *IEEE Trans. Electron Devices*, vol. 30, ED-9, pp. 1123-1134, Sept. 1983.
- [9] E. G. Stevens, "A unified Model of Carrier Diffusion and Sampling Aperture Effects on MTF in Solid-State Image Sensors," *IEEE Trans. Electron Devices*, vol. 39, ED-11, pp. 2621-2623, 1992.
- [10] D. H. Seib, "Carrier Diffusion degradation of modulation Transfer Function in Charge Coupled Imagers," *IEEE Trans. Electron Devices*, vol. 21, ED-3, pp. 210-217, 1974.
- [11] E. G. Stevens, J. P. Lavine, "An Analytical, Aperture and Two-Layer Diffusion MTF and Quantum Efficiency Model for Solid-State Image Sensors," *IEEE Trans. Electron Devices*, vol. 41, ED-10, pp. 1753-1760, 1994.
- [12] J. P. Lavine, W. Chang, C.N. Anagnosyopoulos, B. C. Burkey and E. T. Nelson, "Monte Carlo Simulation of the Photoelectron Crosstalk in Silicon Imaging Devices," *IEEE Trans. Electron Devices*, vol. 32, ED-10, pp. 2087-2091, 1985.
- [13] D. Kavaldjiev, Z. Ninkov, "Subpixel Sensitivity Map for a Charge Coupled Device sensor," *Optical Engineering*, vol. 37, no. 3, pp. 948-954, Mar. 1998.
- [14] S. G. Chamberlain and D. H. Harper, "MTF Simulation Including Transmittance Effects of CCD," *IEEE Trans. Electron Devices*, vol. 25, ED-2, pp. 145-154, 1978.
- [15] O. Yadid-Pecht, "The Geometrical Modulation Transfer Function (MTF)- for different pixel active area shapes," *Optical Engineering*, vol. 39, no. 4, pp. 859-865, 2000.
- [16] N. Teranishi, Y. Ishihara, "Smear reduction in the interline CCD image sensor," *IEEE Trans. Electron Devices*, vol. 34, no. 5, pp. 1052-1056, 1987.
- [17] D. Ramey, J. T. Boyd, "Computer Simulation of Optical Crosstalk in Linear Imaging Arrays," *J. Quant. Electron*, vol. 17, pp. 553-556, Apr. 1981.
- [18] H. Wong, "Technology and device Scaling Considerations for CMOS Imagers," *IEEE Trans. Electron Devices*, vol. 43, ED-12, pp. 2131-2142, Dec. 1996.

## 7. LIST OF FIGURES

Figure 1: Layout example of an “L” shaped active area pixel design. Reprinted from O. Yadid-Pecht, “The Geometrical Modulation Transfer Function (MTF)- for different pixel active area shapes,” *Optical Engineering*, vol. 39, no. 4, pp. 859-865, 2000.

Figure 2: Schematic cross-section of several imager sites, with indication of the depletion-region boundaries.

Figure 3: Geometry of the generalized experiment. The solid squares represent the APS subarray. The optical spot (dark filled rectangle) is scanned over the array in a raster fashion within the scanned region (dashed line rectangle).

Figure 4: Plot of the actual measured PSF for the “L” shaped pixel design (after [15]). The lighter the area - the stronger the response.

Figure 5: Plot of the actual measured PSF for the “L” shaped pixel design (after [15]). Cross-sections used for fitting are located along the arrows, normal to the layout surface. The lighter the area - the stronger the response.

Figure 6: Functional analysis of the obtained Point Spread Function. The example corresponds to the A'-A'' cross-section on Fig. 5.

Figure 7: Mean and standard deviation dependence on the kernel matrix dimensions.

Figure 8: The MTF contour plot calculated from the PSF obtained by laser scanning of the “L” shaped pixel design (after [15]).

Figure 9: The PSF obtained from the unified model for the “L” shaped pixel design. The lighter the area - the stronger the response.

Figure 10: Contour plot of the MTF simulation result for the “L” shaped pixel design.

Figure 11a: The difference between the pure geometrical PSF and the PSF obtained by scanning the “L” shaped pixel design. The lighter the area - the stronger the response (maximum difference ~20% of maximum pixel response).

Figure 11b: The difference between the unified model PSF and the PSF obtained by scanning the “L” shaped pixel design. The lighter the area - the stronger the response (maximum difference ~3% of maximum pixel response).

Figure 12a: The histogram corresponding to the difference obtained in Fig. 11a. The horizontal axis represent this difference as part of the maximum response (which is normalized to unity).

Figure 12b: The histogram corresponding to the difference obtained in Fig. 11b. The horizontal axis represent this difference as part of the maximum response (which is normalized to unity).

Table 1: Parameters comparison.

Fig 1. Layout example of an “L” shaped active area pixel design. Reprinted from O. Yadid-Pecht, “The Geometrical Modulation Transfer Function (MTF)- for different pixel active area shapes,” *Optical Engineering*, vol. 39, no. 4, pp. 859-865, 2000.

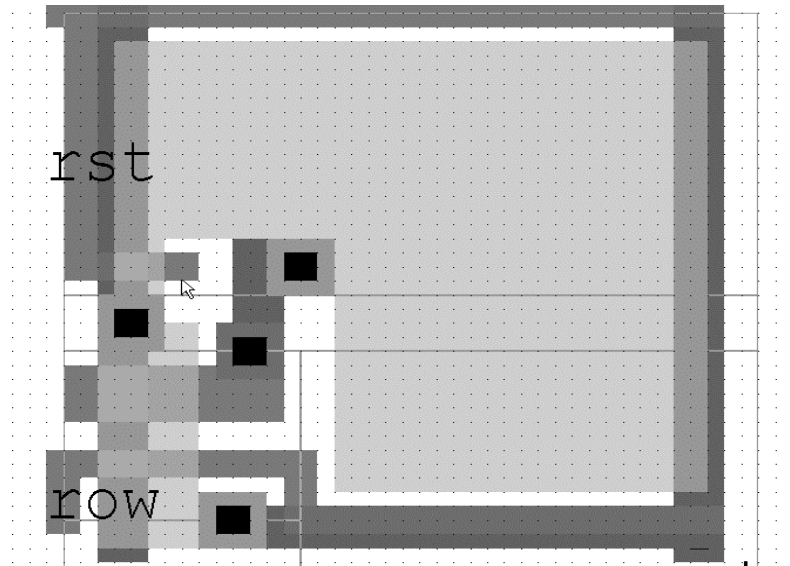


Fig.2. Schematic cross-section of several imager sites, with indication of the depletion-region boundaries.

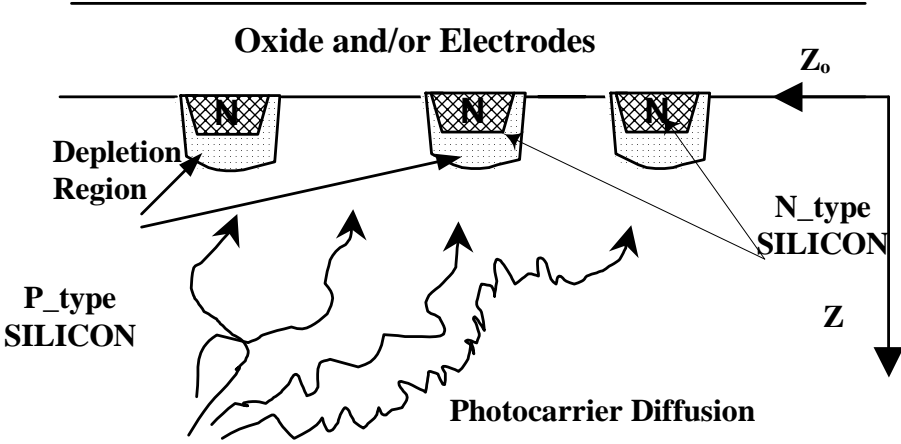


Fig.3. Geometry of the generalized experiment. The solid squares represent the APS subarray. The optical spot (dark filled rectangle) is scanned over the array in a raster fashion within the scanned region (dashed line rectangle).

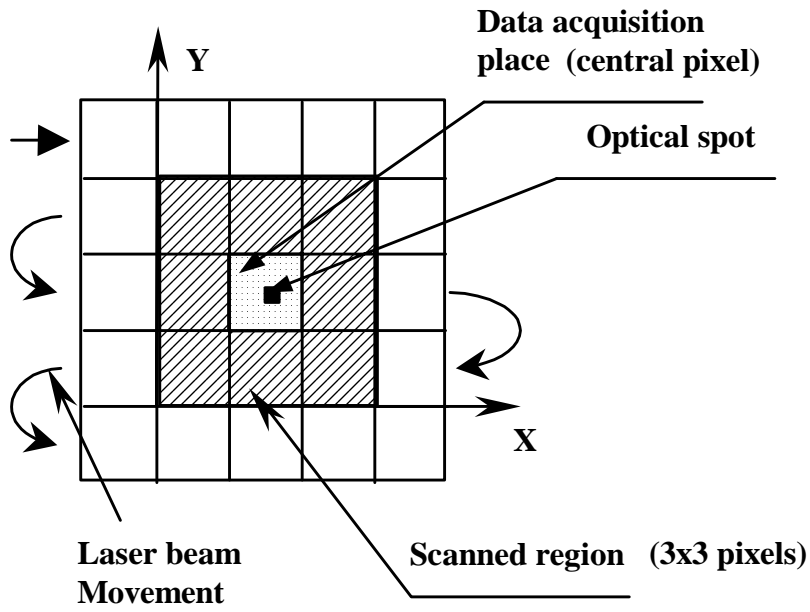


Fig. 4: Plot of the actual measured PSF for the “L” shaped pixel design (after [15]).

The lighter the area - the stronger the response.

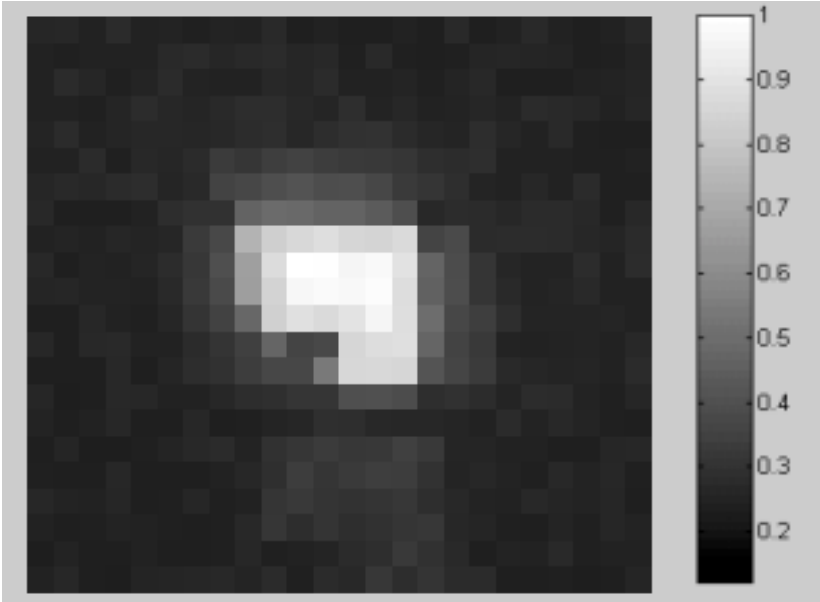


Fig. 5. Plot of the actual measured PSF for the “L” shaped pixel design (after [15]). Cross-sections used for fitting are located along the arrows, normal to the layout surface. The lighter the area - the stronger the response, in correspondence to the Fig. 4.

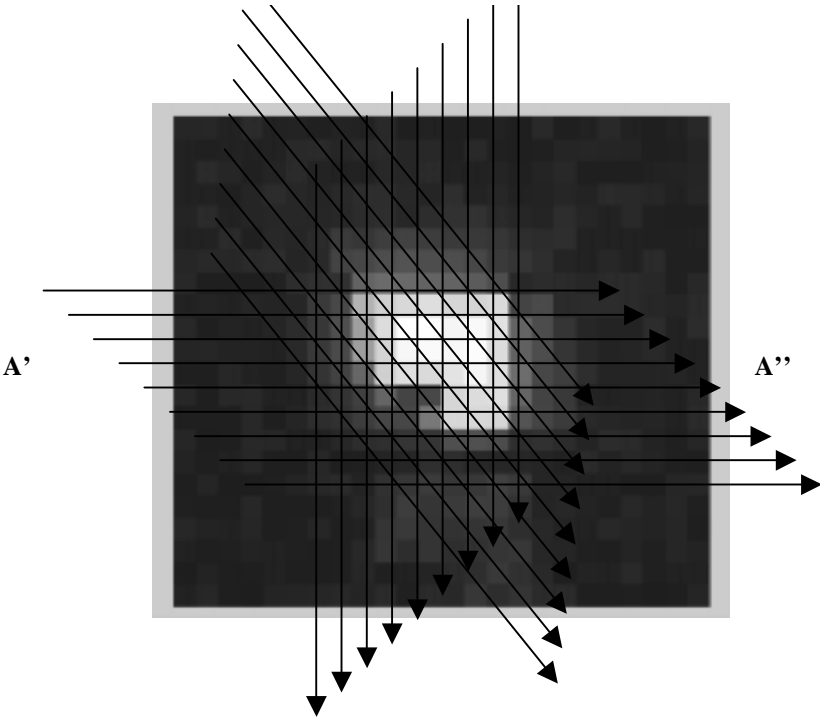


Fig. 6. Functional analysis of the obtained Point Spread Function. The example corresponds to the A'-A'' cross-section on Fig. 5.

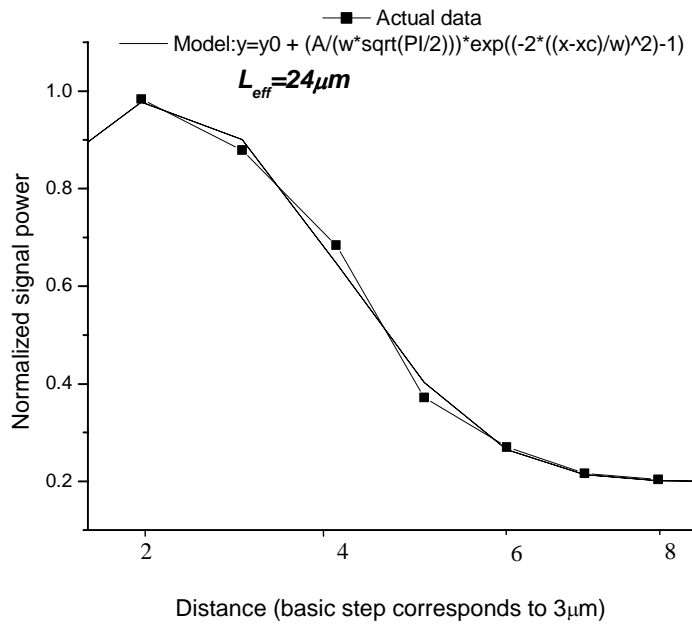


Fig. 7. Mean and standard deviation dependence on the kernel matrix dimensions.

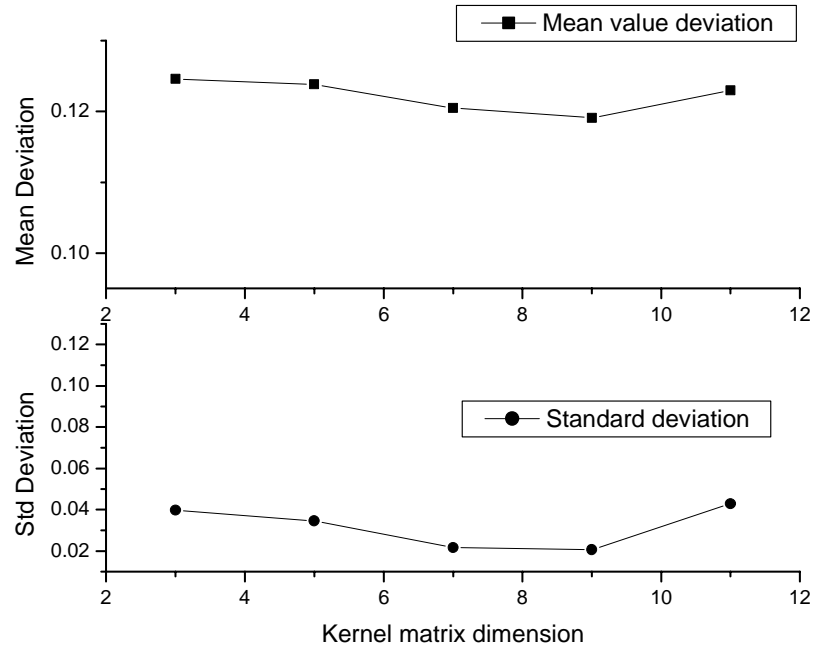


Fig. 8. The MTF contour plot calculated from the PSF obtained by laser scanning of the “L” shaped pixel design (after [15]).

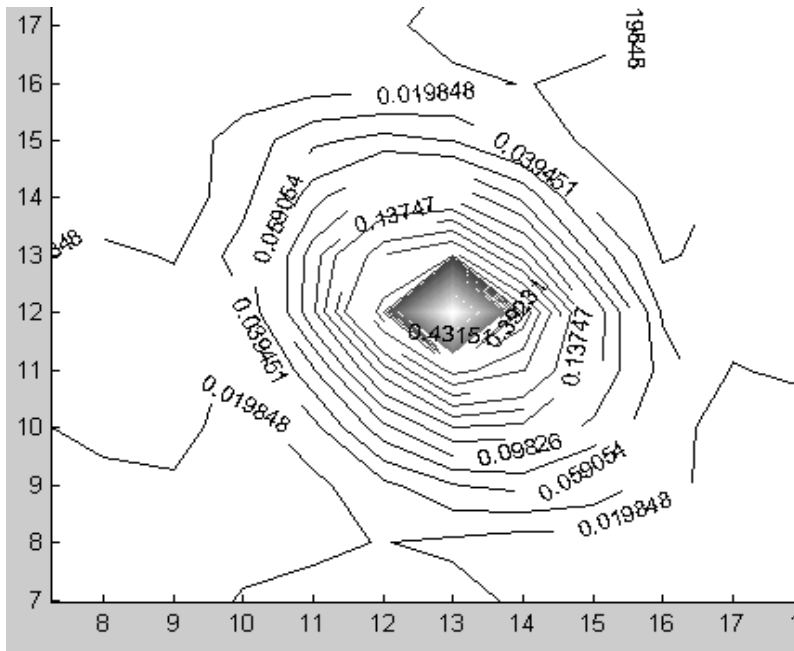


Fig. 9. The PSF obtained from the unified model for the “L” shaped pixel design. The lighter the area - the stronger the response.

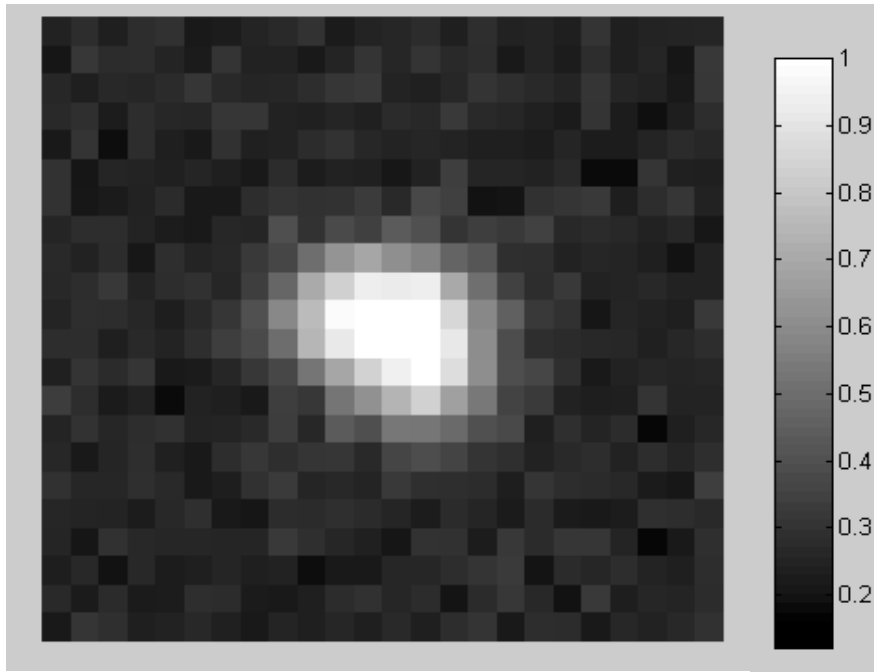


Fig. 10. Contour plot of the MTF simulation result for the “L” shaped pixel design.

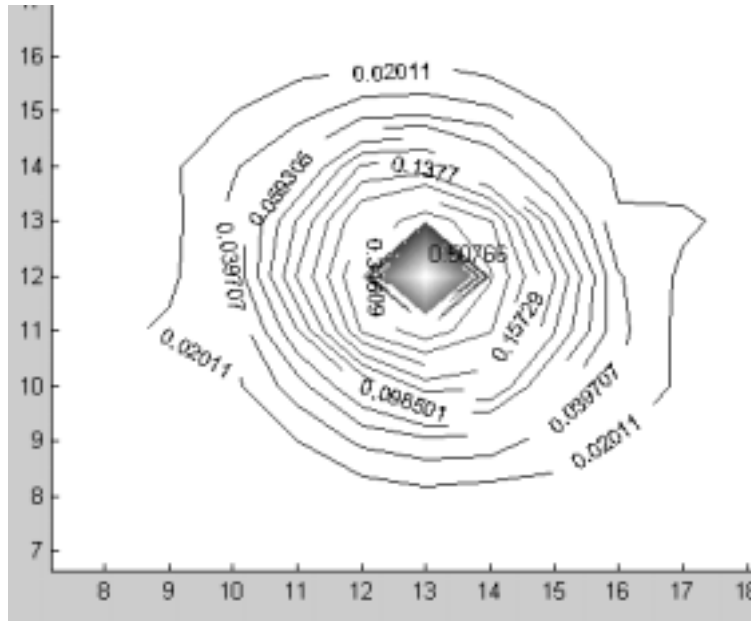


Fig. 11a The difference between the pure geometrical PSF and the PSF obtained by scanning the "L" shaped pixel design. The lighter the area - the stronger the response (maximum difference ~20% of the maximum pixel response).

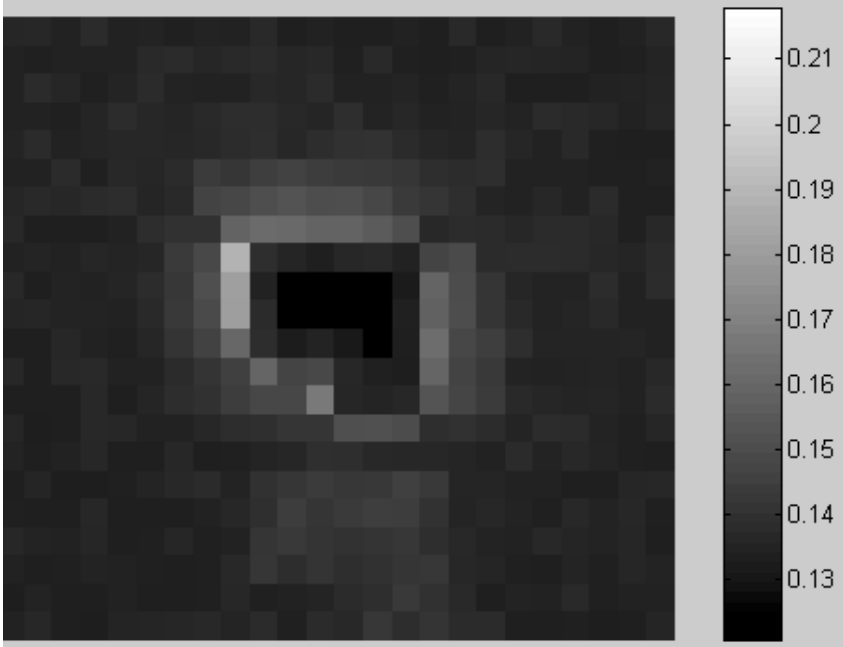


Fig. 11b. The difference between the unified model PSF and the PSF obtained by scanning the "L" shaped pixel design. The lighter the area - the stronger the response (maximum difference ~3% of the maximum pixel response).

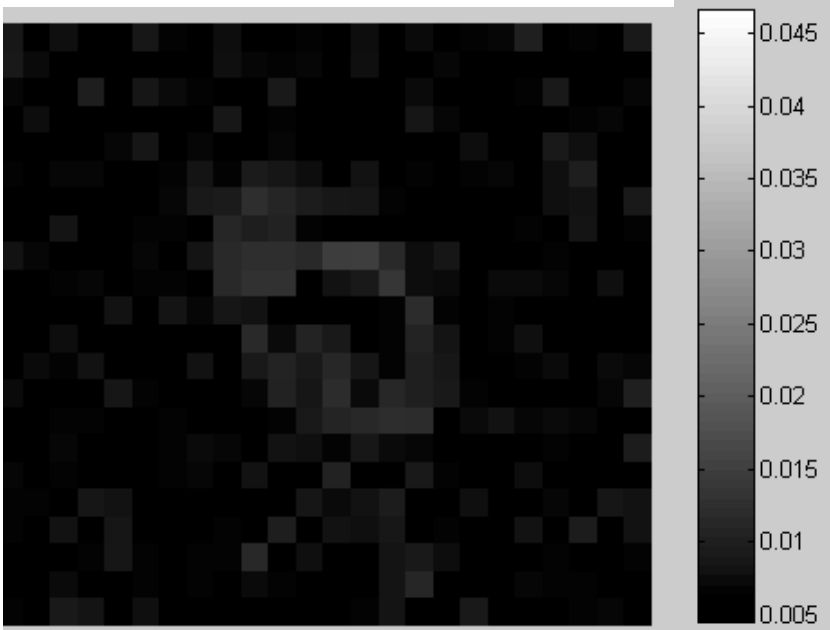


Fig. 12a. The histogram corresponding to the difference obtained in Fig. 11a. The horizontal axis represent this difference as part of the maximum response (which is normalized to unity).

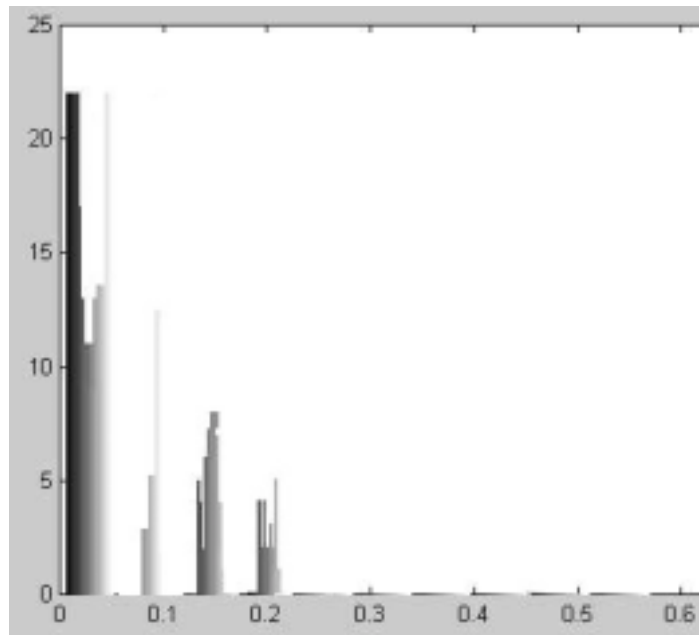


Fig. 12b. The histogram corresponding to the difference obtained in Fig. 11b. The horizontal axis represent this difference as part of the maximum response (which is normalized to unity).

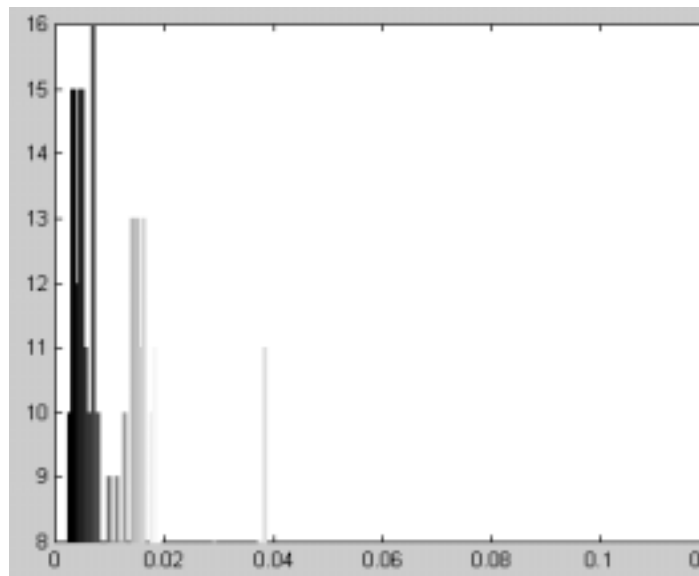


TABLE 1  
PARAMETERS COMPARISON

Diffusion Length	Obtained Value ( $\mu\text{m}$ )
Extracted by Function fits	~24
Extracted from Kernel optimization	~24.4
Calculated: $L_{eff} = \sqrt{D_n \tau}$ , ( $D_n = 37.5 \text{ cm}^2/\text{sec}$ (300K) [2], $\tau = 20 \text{ psec}$ [5])	~27